

On Neural Learnability of Chaotic Dynamics

Ziwei Li* and Sai Ravela

*Earth Signals and Systems Group, Department of Earth, Atmospheric,
and Planetary Sciences, Massachusetts Institute of Technology, Cambridge, MA 91106, USA*

(Dated: March 22, 2022)

In modeling nonlinear dynamics, neural networks are of interest for prediction and uncertainty quantification. The “learnability” of chaotic dynamics by neural networks, however, remains poorly understood. In this work, we show that a parsimonious network trained on few data points suffices for accurate prediction of local divergence rates on the whole attractor. To understand neural learnability, we decompose the mappings in the neural network into a series of geometric stretching and compressing operations that indicate topological mixing and, therefore, chaos. This reveals that neural networks and chaotic dynamical systems are structurally similar, which yields excellent reproduction of local divergence rates. To build parsimonious networks, we employ an approach that matches the spectral features of the dynamics of deep learning those of polynomial regression.

Introduction – Chaotic systems are ubiquitous [24]. For these systems, there usually exists a set of continuous nonlinear governing equations, but finding the exact solutions is often impossible, in part due to a common chaos characteristic wherein two close by trajectories diverge exponentially. In practice, modelers use discretization to solve the nonlinear equations, and often from multiple initial conditions to quantify errors. Doing so, however, raises difficult challenges in the form of non-linearity, high-dimensionality and non-Gaussian uncertainty [21]. As a result, the search for simple-yet-effective models for chaotic dynamics remains a crucial pursuit in the physical sciences.

Recently, there has been a surge of interest in using neural networks (NNs) to emulate chaotic dynamics [2, 3, 7, 9, 19, 29, 30, 32], showing neural networks as promising models. We follow this line of investigation, first showing that neural models with only a few neurons, and trained using a small number of data points, reconstruct the entire attractor object of the classic Lorenz-63 (L63) system [18]. NNs can “extrapolate” from partial knowledge of the attractor, rendering a uniform distribution of the training data unnecessary. The neural models are also, it appears, as chaotic as the L63 system they train from.

This success is much like other effort seeking to emulate chaotic dynamics. By way of explanation, one typically resorts to the universal approximation theorem (UAP) [10, 16, 17, 23]. However, UAP is an existence statement. It neither explains the emergence of chaos nor the efficacy with which the attractor is reconstructed. Inspired by the validity of a geometric interpretation of the L63 system [26], we show that a geometric perspective helps to explain the neural efficacy. Neural mappings alternately rotate, stretch, and compress, which are the defining characteristics of chaotic dynamics [6]. Whilst the question of optimizing neural computation for prediction remains open, our work suggests that possession of

geometrical properties required by chaos theory enables neural networks to efficiently match the structure of the L63’s attractor object and its predictability. To the best of our knowledge, this explanation for neural learnability of chaos is new [20]. A key step in this process is to show that NNs are compact and do not over-fit in relation to the attractor object. We achieve this by noting that L63 is a polynomial, allowing us impose bounds the size of the neural network [22, 25].

Methods – The L63 model was originally used to describe 2-D Rayleigh-Bénard convection, in which the parameters of the streamfunction and temperature fields are written in a set of ordinary differential equations [18]:

$$\begin{aligned}\dot{X} &= \sigma(Y - X); \\ \dot{Y} &= \rho X - Y - XZ; \\ \dot{Z} &= -\beta Z + XY,\end{aligned}\tag{1}$$

where X and Y are the strengths of the streamfunction and temperature modes, and Z represents the deviation of the vertical temperature profile from linearity. Consistent with Lorenz’s original paper, we set $\sigma = 10$, $\beta = 8/3$, and $\rho = 28$. The solutions of L63 are known to be dissipative (volume in phase space contracts rapidly), and chaotic (sensitive to initial perturbations).

We define L63 as a discrete mapping from the current state of the system $\mathbf{x}_n = (X, Y, Z)^T$ to the state of the next timestep \mathbf{x}_{n+1} :

$$\Phi_{L63}(\mathbf{x}_n) = \mathbf{x}_{n+1}.\tag{2}$$

We choose this discrete form both for L63 and NN maps because it provides a straightforward connection between the geometric L63 mapping and dynamics in the neural network. Since the exact form of Eq. (2) for L63 is unknown, the discrete map is obtained by numerically integrating Eq. (1) and sampling at increment dt .

The discrete map implemented by a single-hidden-layer feedforward NN is

$$\Phi_{NN}(\mathbf{x}_n) = \mathbf{W}_2 g(\mathbf{W}_1 \mathbf{x}_n + \mathbf{b}_1) + \mathbf{b}_2,\tag{3}$$

in which the 3×1 input vector, \mathbf{x}_n , is first left-multiplied by an $L \times 3$ weight matrix \mathbf{W}_1 , and added to an $L \times 1$

* ziweili@mit.edu

bias term \mathbf{b}_1 , where L is the number of neurons. The resulting vector is then element-wise ‘‘compressed’’ by a sigmoid function g , which takes the form of \tanh in our setup. Left-multiplication by a $3 \times L$ matrix \mathbf{W}_2 followed by addition of another bias term \mathbf{b}_2 finishes a mapping iteration of the NN.

We use Matlab function *ode45* to numerically solve for the discrete mappings of L63 as training data. To obtain data on the attractor, we randomly initialize 1000 trajectories from region $[-20, 20] \times [-20, 20] \times [0, 50]$ with uniform distribution. Each trajectory is integrated for 2500 timesteps with $dt = 0.01$. We abandon the first 2000 timesteps to remove the transient parts, which are much shorter than 2000 steps. Then, the remaining 500 timesteps of the 1000 trajectories are aggregated as pairs $(\mathbf{x}, \mathbf{x}')$ that satisfy $\mathbf{x}' = \Phi_{L63}(\mathbf{x})$, forming the training data pool.

The prior locations of the training data pairs (\mathbf{x}) can be seen as a representation of the L63 attractor (\mathcal{A}_{L63}), and each consecutive location pair provide information about the discrete L63 flow. We then randomly sample a specific number of training pairs from the data pool to train NNs. Each NN is trained for 10^3 epochs with Bayesian regularization [8], where an epoch means a full sweep through the sampled training data.

We use the finite-time Lyapunov exponent (FTLE) [13] to compare the local divergence rates of NN and L63 and quantify their similarity on the basis of predictability. The FTLE is computed from forward-propagating two nearby trajectories that originate from the vicinity of the \mathcal{A}_{L63} attractor. Formally, it is defined as

$$\lambda_{\max} := \frac{1}{N_t} \ln \frac{\max_{\delta \mathbf{x}_0} |\delta \mathbf{x}_{N_t}|}{|\delta \mathbf{x}_0|} = \frac{1}{N_t} \ln \sqrt{\sigma_{\max}}, \quad (4)$$

where λ_{\max} denotes the maximum FTLE, $\delta \mathbf{x}_0$ is the initial perturbation between two trajectories, and $\delta \mathbf{x}_{N_t}$ denotes their difference after N_t steps. The FTLE relates to the original Lyapunov exponent when $N_t \rightarrow \infty$ and $\delta \mathbf{x}_0 \rightarrow 0$ [4]. To obtain λ_{\max} , we select the direction of $\delta \mathbf{x}_0$ such that $|\delta \mathbf{x}_{N_t}|$ is maximized, and in practice, we calculate λ_{\max} using the largest eigenvalue (σ_{\max}) of $\mathbf{J}^T \mathbf{J}$, where \mathbf{J} is the Jacobian matrix evaluated using perturbations around \mathbf{x}_0 .

Results – We first show that NN can learn the chaotic dynamics of L63 efficiently with a small number of data and neurons. The quadratic prediction error is reported in Ref. [31], and will not be the main focus of this paper. We instead compare the short-term and long-term behaviors of the two systems. Specifically, we show that the dynamics represented by NN possess similar predictability to L63 as quantified by FTLE, and NNs are able to extrapolate regions that are unknown in the training data.

We analyze a 4-neuron network trained on 40 data points randomly sampled from the training data pool (table I shows the learnt parameters of this network). Fig. 1 depicts two trajectories that follow the L63 flow

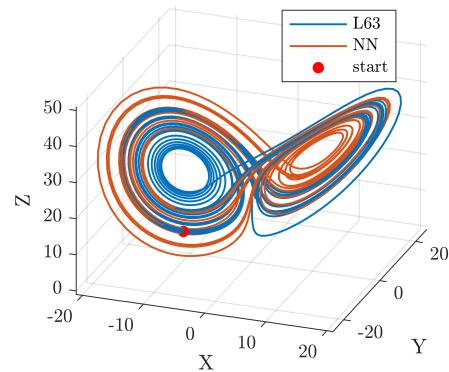


FIG. 1. Two trajectories produced by L63 (blue) and the 4-neuron NN trained on 40 data points sampled from the whole attractor (red). They are both 2000 timesteps long, and start from the same location on the Lorenz attractor.

and the flow of the trained NN, respectively. They interlace with each other, creating the well-known Lorenz attractor. Trajectories starting from other locations on the attractor roughly trace out the same structure (not shown). The close-resemblance between the two attractors indicates that the dynamics of this parsimonious NN is similar to that of L63, i.e., NNs are able to learn chaotic dynamics efficiently.

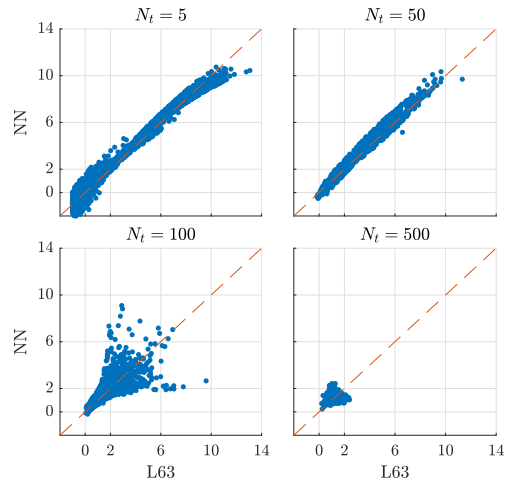


FIG. 2. One-to-one scatter plot of FTLE with NN and L63. The NN used in this plot has 4 neurons and is trained on only 40 data points. The panels correspond to four integration steps, N_t , with time increment $dt = 0.01$.

To calculate FTLE, we generate points following the NN flow using the same generation process as in *Methods*. The generated points in the phase space represents the NN attractor (\mathcal{A}_{NN}). We then randomly initialize 2000 trajectories on \mathcal{A}_{L63} . Every trajectory from \mathcal{A}_{L63} is paired with another trajectory that starts from the closest point on \mathcal{A}_{NN} , and in each pair of trajectories, the former follows the L63 flow while the latter follows the NN flow.

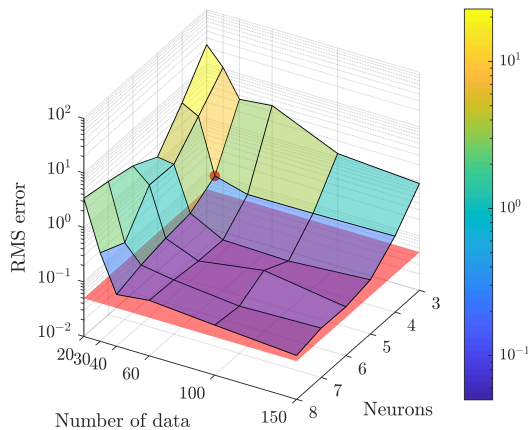


FIG. 3. The root-mean-square error in FTLE of neural networks for each neuron and number-of-data configuration. The FTLE is calculated with $N_t = 50$ and averaged over 2000 trajectories randomly initialized on the attractor. The red dot represents the example configuration in Fig. 1 and 2. The red surface is located at $z = 0.05$.

The FTLE of the trajectory pairs are compared under different timesteps: $N_t = 5, 50, 100, 500$ (Fig. 2). When $N_t = 5, 50$, NN accurately reproduces local divergence rates over the whole attractor, indicating that the short-term predictability of the two systems agree with each other. As N_t increases, the correspondence diverges ($N_t = 100$), and converges again ($N_t = 500$) to the classical largest Lyapunov exponent of L63, which is roughly 0.91 as in Ref. [28]. The convergence of FTLE under large timesteps implies that the long-term behavior of the two systems is also similar.

TABLE I. Parameters of the 4-neuron NN flow

Matrix	Values			
\mathbf{W}_1	0.0034	0.0030	-0.0050	
	0.0115	0.0072	-0.0015	
	-0.0067	-0.0009	-0.0064	
	-0.0075	-0.0005	0.0001	
\mathbf{b}_1^T	-0.1131	-0.6111	-0.0266	-0.1395
\mathbf{W}_2	6.0807	5.2861	-7.9178	-107.1371
	370.0114	-26.1875	-270.5582	366.2765
	-169.8626	95.5298	-40.6654	62.2099
\mathbf{b}_2^T	-11.5557	71.0935	40.1989	
diag(\mathbf{S})	4.3852	1.2087	0.7184	0.0000

The agreement in FTLE generally improves under increasing numbers of neurons and data points (Fig. 3). This trend is expected if we invoke the bias and variance trade-off [11]: increased complexity in learning models such as neural networks generally translates into better prediction accuracy (lower bias), provided that regularization techniques prevent the learning algorithm from entering the high-variance regime.

NN can extrapolate from an incomplete training dataset. Fig. 4 shows a comparison of two trajec-

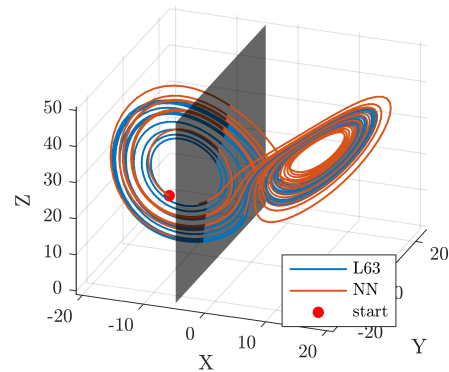


FIG. 4. Similar to Fig. 1, but the red trajectory is produced by a 5-neuron NN trained on 100 data points sampled from $X > -5$ part of the attractor. The region to the right of the grey partition is the training data range, and the region to the left is unknown to the NN.

ries predicted by NN and L63 that originate from the same location (red dot). The NN in this case has 5 neurons, and is trained on 100 data points sampled from the $X > -5$ part of \mathcal{A}_{L63} , which amounts to knowing 73% of the attractor structure. The two trajectories are close in the first 100 timesteps, and then bifurcate onto the two branches of the attractor. Despite starting from an unknown region, the NN still predicts a well-behaved attractor that closely resembles the original attractor in the extrapolated region of $X \leq -5$. The one-to-one correspondence of FTLEs between L63 and the NN trained on the incomplete dataset is similar to Fig. 2 (not shown).

Geometric perspective of the NN flow – We showed from the previous section that the neural learnability on the L63 dynamics is very good. However, the theoretical approach to understand this learnability is unknown. Although the UAP states that mapping Φ_{L63} can be approximated by NN arbitrarily well, it does not explain the NN’s ability to reconstruct the strange attractor efficiently, nor its skill of extrapolation. Inspired by the exact mathematical correspondence between the geometric Lorenz flow and L63 [12, 26], we give our geometric understanding of the NN flow.

The dynamics of NN (Eq. 3) can be seen as a mapping in a multi-dimensional Riemann space (this interpretation is also used in classification problems [14]). In the discrete map of the simple 4-neuron network discussed above, the input vector \mathbf{x} in the 3-D phase space is mapped into a 4-D *neuron space*, and then mapped back to the phase space. We write an N_t -step trajectory ($N_t \geq 2$) as $\mathcal{L}_0^{N_t} = \{\mathbf{x}_0, \mathbf{x}_1, \dots, \mathbf{x}_{N_t}\}$. In each mapping from step $n \rightarrow n+1, n \in \{0, 1, \dots, N_t-1\}$, there exists a 4-D intermediate vector \mathbf{y} in the neuron space:

$$\mathbf{y}_{n+1} = g(\mathbf{W}_1 \mathbf{x}_n + \mathbf{b}_1), \quad (n = 0, 1, \dots, N_t - 1). \quad (5)$$

We refer to \mathbf{y} as *neuron vector*. The recurrence relation of the neuron vector is then:

$$\mathbf{y}_{n+1} = g(\mathbf{W}^* \mathbf{y}_n + \mathbf{b}^*), \quad (n = 1, 2, \dots, N_t - 1). \quad (6)$$

where $\mathbf{W}^* = \mathbf{W}_1\mathbf{W}_2$ is a 4-by-4 matrix, and $\mathbf{b}^* = \mathbf{W}_1\mathbf{b}_2 + \mathbf{b}_1$ is a 4-by-1 vector. \mathbf{W}^* can be decomposed as $\mathbf{W}^* = \mathbf{U}\mathbf{S}\mathbf{V}^T$ using singular-value decomposition. \mathbf{U} and \mathbf{V} are 4-D both orthonormal matrices, and \mathbf{S} is a diagonal matrix of rank 3. We then rewrite Eq. (6) more explicitly as

$$\mathbf{y}_{n+1} = g(\mathbf{U}\mathbf{S}\mathbf{V}^T\mathbf{y}_n + \mathbf{b}^*), \quad (7)$$

which we call the *neuron map*. Equation (7) encodes the entire dynamics learnt by NN, because it is different from Eq. (3) by a homomorphism, i.e., Eq. (5). Therefore, understanding the neuron map is equivalent to understanding the dynamics of NN.

The neuron map comprises 4 sub-steps: rotation, stretch, rotation, and compression. *Rotations* in this paper takes the generalized sense of orthogonal transformation, and they are carried out by matrices \mathbf{V}^T and \mathbf{U} in the neuron map. Since the sigmoid function only has a compressing effect due to its gradient being smaller than or equal to 1, diagonal matrix \mathbf{S} must have at least one diagonal element larger than 1 in order to satisfy the requirement of stretching in chaotic dynamics. For the 4-neuron NN at question, \mathbf{S} imposes expanding effect in two dimensions since two of its diagonal elements are greater than 1 (see table I).

Through the error growth between each timestep, the effects of compression and expansion exerted by NN are seen more clearly. For a small perturbation ($\delta\mathbf{y}$) between two initial points near \mathbf{y} , its value at the next timestep is

$$\delta\mathbf{y}' = g'(\mathbf{W}^*\mathbf{y} + \mathbf{b}^*) \odot \mathbf{W}^*\delta\mathbf{y} \quad (8)$$

where we neglected second- and higher-order terms, and \odot denotes the element-wise product. We let $G_{jj} = g'(\sum_{i=1}^L W_{ji}^*y_i + b_j^*)$, then $g'(\mathbf{W}^*\mathbf{y}_n + \mathbf{b}^*) \odot \mathbf{W}^*\delta\mathbf{y} = \mathbf{G}\mathbf{W}^*\delta\mathbf{y}$, where $\mathbf{G} = \text{diag}\{G_{11}, G_{22}, \dots\}$. The squared error is then

$$|\delta\mathbf{y}'|^2 = (\mathbf{W}^*\delta\mathbf{y})^T \mathbf{G}^2 \mathbf{W}^* \delta\mathbf{y}. \quad (9)$$

From Eq. (9), it's clear that singular values of \mathbf{W}^* that are larger than 1 will expand the perturbation, and \mathbf{G} compresses the perturbation since $g'(x) \in (0, 1]$, $\forall x \in \mathbb{R}$. With information of \mathbf{y} , \mathbf{G} controls the degree of compression in each direction in the neuron space. \mathbf{U} and \mathbf{V} in the decomposition of \mathbf{W}^* controls the orientations of compression and expansion, so that they take place in different directions.

The stretch and compression sub-steps in neuron maps are frequently thought of as the standard way to create topological mixing, an indicator of chaos. The ability to be trained to obtain these geometric operations makes NN very good to approximate discrete chaotic mapping. As another perhaps more concrete example, a 2-neuron NN map can be trained to faithfully recreate the Hénon NN map (not shown), which is a 2-D chaotic map defined

such that trajectories are stretched in one direction and compressed in the other [15].

Generalization to multi-layer networks is straightforward in the above framework. Since “the dynamics of the neural vector” will be ambiguous as there are multiple layers of neurons, we apply the same argument to perturbations in the phase space. For a perturbation of $\delta\mathbf{x}$ around \mathbf{x} , its squared length at the next timestep is

$$|\delta\mathbf{x}'|^2 = |\mathbf{W}_{N+1}\mathbf{G}_N\mathbf{W}_N\dots\mathbf{G}_1\mathbf{W}_1\delta\mathbf{x}|^2, \quad (10)$$

where $\mathbf{G}_i = \text{diag}\{g'(\mathbf{W}_i\mathbf{y}_{i-1} + \mathbf{b}_i)\}$, and \mathbf{y}_{i-1} is the neuron vector of the i th layer for $i > 1$ ($\mathbf{y}_0 = \mathbf{x}$). The weight and gradient matrices then consecutively parameterize multiple stretching and compressing operations in a single NN map.

Lower-bounding the number of neurons – Since the Euler-forward scheme of Eq. (1) is a 3-D ($n = 3$) polynomial with a degree of at most $d = 2$, we use previous theoretical results on learning polynomials with NNs [1, 5] to establish lower bounds on the necessary number of neurons. In effect, we assume that the dynamics are polynomial but the learning system doesn't know the exact governing equations. The number of neurons (L) for learning a polynomial with root-mean-square error target ϵ is bounded by $L = \Omega(n^{6d}/\epsilon^3)$ [1]. This is a rather coarse estimate as more than 5×10^5 nodes are needed when $\epsilon \sim 1$. In stark contrast, exactly two neurons in a single hidden-layer of a PolyNet reproduce the sparse L63 polynomial to numerical precision [25]. Matching equilibrium norms of neural and polynomial regression asymptotically, a full polynomial (n, d) needs $L = \binom{n+d}{d} - (n+1)$ hidden nodes [22, 25] for an exact match. If a polynomial were instead represented by a network with direct input-output connections for the linear part, added with a single tanh-activated hidden-layer for the residual nonlinear part, then matching the equilibrium norm yields a bound: $L \propto \frac{n}{2n+1} \left[\binom{n+d}{d} - (n+1) \right]$ of hidden-layer units [22]. Eliminating constants using random bounded-input, bounded-weight networks reveals that an $n = 3, d = 2$ polynomial matches networks of 3 to 8 nodes with 95% confidence. Note that the standard network with just a single hidden tanh-layer with no input-output bypass is sub-optimal, asymptotically yielding the bound [22]: $L \propto \frac{n}{2n+1} \left[\binom{n+d}{d} - 1 \right]$ of hidden-layer units.

A Taylor-expansion of the sigmoid function to the third order: $\tanh(x) = x - x^3/3 + O(x^5)$ allows Eq.(3) to be modeled as a polynomial of degree 3 (NN polynomial). We further require all coefficients of the NN polynomial to be equal to those in Eq. (1). Then for an NN with L hidden nodes, biases, and n -dimensional input/output, a total of $2nL + n + L$ parameters should satisfy $3C_{(n+3)}^3$ constraining equations. The parameters should be over-determined for a good fit, hence at least $L = \lceil (3C_{(n+3)}^3 - n)/(2n+1) \rceil = 9$ hidden nodes are needed. To obtain an error estimate, we assume that the prediction errors between NN and its truncated polynomial dominates over the errors between NN and L63,

therefore the truncation errors of NN polynomial provides an upper bound on the prediction error of NN. We can estimate the truncation error by substituting table I into the NN polynomial to obtain $\Phi_{\text{NN-poly}}$, and calculate the expected error over data sampled from the \mathcal{A}_{NN} attractor: $\epsilon^2 = \langle (\Phi_{\text{NN-poly}} - \Phi_{\text{NN}})^2 \rangle_{\mathcal{A}_{\text{NN}}}$. 5000 random samples on \mathcal{A}_{NN} gives a normalized error of $\epsilon \sim 0.12$.

Discussion – Our work suggests that NN may be a good candidate to learn from data and represent a broad range of chaotic dynamics with a good skill of generalization. With the flow-like dynamics and gradient-descent algorithm, it may serve as a non-parametric model for chaotic systems without explicit expressions. Conversely, neural networks can be seen as a much more generalized class of chaotic systems. Apart from compression and expansion operations that are necessary for chaos, the higher-dimensional rotations are also vital in creating the flow-like dynamics. We may further posit that the neu-

ral networks may be a unifying formulation for modeling chaotic dynamics because it reproduces the Hénon map and the discrete Lorenz map under the same mathematical framework.

On the other hand, the compression operation represented by the sigmoid function makes NN preferable to model simple dissipative systems; its ability to model conservative dynamics and systems of much higher dimensions is yet to be tested. More work is also needed, possibly with the aid of Riemann geometry, to fundamentally understand the geometric operations in the high-dimensional neuron space.

Acknowledgments – Ziwei Li was advised by Sai Ravela. Support from ONR grant N00014-19-1-2273, the MIT Environmental Solutions Initiative, the John S. and Maryann Montrym Fund, and the MIT Lincoln Laboratory is gratefully acknowledged.

-
- [1] Andoni, A., Panigrahy, R., Valiant, G., and Zhang, L., in *Proceedings of the 31st International Conference on International Conference on Machine Learning* (2014).
- [2] Bahi, J. M., Couchot, J. F., Guyeux, C., and Salomon, M., *Chaos* **22**, 013122 (2012).
- [3] Bakker, R., Schouten, J. C., Lee Giles, C., Takens, F., and Van den Bleek, C. M., *Neural Computation* **12**, 2355 (2000).
- [4] Barreira, L. and Pesin, Y., in *University Lecture Series*, Vol. 23 (American Mathematical Society, Providence, RI, 2002) p. 151.
- [5] Barron, A. R., *IEEE Transactions on Information Theory* **39**, 930 (1993).
- [6] Berge, P., Pomeau, Y., and Vidal, C., *Order within chaos* (Wiley, 1987) p. 329.
- [7] Chen, R. T., Rubanova, Y., Bettencourt, J., and Duvenaud, D., in *32nd Conference on Neural Information Processing Systems* (2018).
- [8] Dan Foresee, F. and Hagan, M. T., in *Proceedings of International Conference on Neural Networks* (1997).
- [9] Dudul, S. V., *Applied Soft Computing* **5**, 333 (2005).
- [10] Funahashi, K. and Nakamura, Y., *Neural Networks* **6**, 801 (1993).
- [11] Goodfellow, I., Bengio, Y., and Courville, A., *Deep Learning* (MIT Press, Cambridge, MA, 2016).
- [12] Guckenheimer, J. and Williams, R. F., *Publ. Math. IHES* **50**, 307 (1979).
- [13] Haller, G., *Physica D: Nonlinear Phenomena* **149**, 248 (2001).
- [14] Hauser, M. and Ray, A., in *31st Conference on Neural Information Processing Systems* (2017) p. 10.
- [15] Hénon, M., *Communications in Mathematical Physics* **50**, 69 (1976).
- [16] Hornik, K., *Neural Networks* **4**, 251 (1991).
- [17] Hornik, K., Stinchcombe, M., and White, H., *Neural Networks* **2**, 359 (1989).
- [18] Lorenz, E. N., *Journal of the Atmospheric Sciences* **20**, 130 (1963).
- [19] Madondo, M. and Gibbons, T., in *Proceedings of the Midwest Instruction and Computing Symposium* (2018).
- [20] The term learnability is used here in the sense of neural system’s fidelity to specified properties of a dynamical system, e.g., the predictability of the dynamical system quantified by finite-time Lyapunov exponent. This is somewhat different from Valiant’s definition [27].
- [21] Ravela, S., “Tractable non-gaussian representations in dynamic data driven coherent fluid mapping,” in *Handbook of Dynamic Data Driven Applications Systems*, edited by E. Blasch, S. Ravela, and A. Aved (Springer International Publishing, Cham, 2018) pp. 29–46.
- [22] Ravela, S., Li, Z., Trautner, M., and Reilly, S., Preprint (2019).
- [23] Seidl, D. R. and Lorenz, R. D., in *Proceedings of the International Joint Conference on Neural Networks 1991*, Vol. 2 (IEEE, 1991) pp. 709–714.
- [24] Strogatz, S. H., *Nonlinear Dynamics and Chaos: With Applications to Physics, Biology, Chemistry, and Engineering*, 2nd ed. (CRC Press, Boca Raton, FL, 2015) p. 531.
- [25] Trautner, M. and Ravela, S., “Neural integration of continuous dynamics,” (2019), arXiv:1911.10309 [cs.LG].
- [26] Tucker, W., *Foundations of Computational Mathematics* **2**, 53 (2002).
- [27] Valiant, L. G., *Commun. ACM* **27**, 1134 (1984).
- [28] Viswanath, D., *Lyapunov Exponents from Random Fibonacci Sequences to the Lorenz Equations*, Ph.D. thesis, Cornell University, Ithaca, NY, USA (1998).
- [29] Yu, R., Zheng, S., and Liu, Y., in *Proceedings of the ICML 17 Workshop on Deep Structured Prediction* (2017).
- [30] Zerroug, A., Terrissa, L., and Faure, A., *Annual Review of Chaos Theory, Bifurcations and Dynamical Systems* **4**, 55 (2013).
- [31] Zhang, L., in *2017 IEEE 30th Canadian Conference on Electrical and Computer Engineering*, 2 (2017) pp. 30–33.
- [32] Zhang, L., in *2017 IEEE Life Sciences Conference* (2017) pp. 39–42.